ELSEVIER

Coastal Engineering 42 (2001) 115–142

Coastal Engineering
An International Journal for Coastal, Harbour and Offshore Engineers

www.elsevier.com/locate/coastaleng

Long-term morphological modeling of a tidal inlet: the Arcachon Basin, France

Florence Cayocca *

Département Recherches Océaniques, Géologie Marine, IFREMER, B.P. 70, 29380 Plouzané, France

Received 18 February 1999; received in revised form 7 February 2000; accepted 5 July 2000

Abstract

The Arcachon Lagoon on the French Atlantic coast is a triangular shaped lagoon of 20 km on a side connected to the ocean by a 3-km wide inlet between the mainland and an elongated sand spit. This tidal inlet exhibits a particularly active morphology due to locally strong tidal currents and rough wave conditions. During the past 300 years, minimum and maximum spatial extents of the Cap Ferret sand spit have varied by 8 km while one or two channels have alternately allowed circulation between the lagoon and the ocean. These impressive morphological changes have never prevented regular flushing of the lagoon, eventhough the spit came as close as 300 m from the coast during the 18th century. According to Bruun's concept of tidal inlet stability [Theory and Engineering (1978), 510 pp.], the balance between longshore littoral transport and the tidal prism ensures the perpetuity of the inlet.

Process modeling was believed to give better insight into the respective roles of tides and waves in driving the long-term morphological changes of the inlet. A two-dimensional horizontal morphodynamic model was therefore developed, combining modules for hydrodynamics, waves, sediment transport and bathymetry updates. The use of process models at a scale of decades requires a schematization of the input conditions. We defined representative mean annual wave and tide conditions with respect to sediment transport, i.e. conditions that induce the same annual transport as measured in the field. Driven by these representative conditions, simulations run from the 1993 bathymetry show that the tide is responsible for the opening of a new channel at the extremity of the sand spit (where tidal currents are the strongest), while waves induce a littoral transport responsible for the longshore drift of sand bodies across the inlet. One particular simulation consisted in running the model from a hypothetical initial topography where the channels are filled with sand and the entire inlet is set to a constant depth (3 m). The results show the reproduction of a channel and bar system comparable to historical observations, which supports the idea that the lagoon is unlikely to be disconnected from the ocean, provided tide and wave conditions remain fairly constant in the following decades.

Keywords: Tidal inlets; Numerical models; Landform evolution; Sediment transport; Longshore current

1. Introduction

Coastal morphodynamic processes around tidal inlets in mixed-energy environments (macrotidal environment of high wave energy, Hayes, 1980) are particularly complex. Severe tide and wave condi-

* Tel.: +33-2-98-22-42-58; fax: +33-2-98-22-45-79.
E-mail address: fcayocca@ifremer.fr (F. Cayocca).

0378-3839/01/$ - see front matter
PII: S0378-3839(00)00053-3

tions produce significant bathymetric changes at time scales varying from hours to decades or centuries. Empirical and conceptual models have increased understanding of the overall mechanisms driving the behavior of these inlets (O'Brien, 1931, 1969; Keulegan, 1951; Bruun, 1978; de Vriend et al., 1993a,b; van Dongeren and de Vriend, 1994) and in particular their inherent instability (Bruun and Gerritsen, 1960; Escoffier, 1977; Bruun, 1978; Fitzgerald, 1988; Gerritsen, 1990; Gao and Collins, 1994; Goodwin, 1996). However, they fail to explain some large-scale morphological changes or cyclic features, and cannot investigate the respective roles of tides and waves in reshaping an inlet.

The rapid evolution of the Arcachon tidal inlet in recent centuries and its quasi-closure in 1826 have instigated several descriptive and conceptual studies in the last 25 years. During the past 300 years, minimum and maximum extents of the sand spit separating the Arcachon lagoon from the ocean have resulted in variations of 8 km, while one or two channels have alternately allowed circulation through the inlet. Similar lagoons were once connected to the ocean further south along the coast. The closure of these lagoons raises the possibility of a similar closure of the Arcachon lagoon. Empirical methods developed to assess the stability of such inlets compare the value of the mean annual littoral transport (representative of the wave action) to the tidal prism of a mean spring tide (Bruun, 1978). According to such relationships, the Arcachon inlet was shown to be stable (Cayocca, 1996). This stability concept does not imply that the inlet morphology is static, but ensures its perpetuity through continuous flushing enabled by the tidal currents. While this approach provides interesting information regarding the overall behavior of the inlet, it does not allow a proper understanding of the mixed processes that drive the detailed evolution and the possible closure of the lagoon.

In the absence of a continuous set of data spanning several years or decades (the typical time-scale of larger morphological changes), developing a process-based morphodynamic model is an interesting attempt to understand the physical processes around the inlet. Morphodynamic models have experienced increasing popularity with the development of more powerful computers. Eventhough some attempts have recently been made to develop quasi- and fully three-dimensional models (Watanabe et al., 1986; Briand and Kamphuis, 1993a,b; Ranasinghe et al., 1999), more attention has been devoted to two-dimensional horizontal models (Coeffé and Péchon, 1982; Watanabe, 1982; de Vriend, 1987a,b; Andersen et al., 1991; Roelvink and van Banning, 1994; Chesher, 1995; Ribberink et al., 1995; Wang, 1991; Wang et al., 1995; Nicholson et al., 1997). Depth averaged schemes cannot account for undertow, wave asymmetry or curvature-induced secondary flows; their application is therefore restricted to areas where these processes can be disregarded (unless they can be modeled separately through a quasi-3D approach), or where longshore processes are dominant over cross-shore processes. Since morphological evolutions in the Arcachon tidal inlet are thought to depend mostly on the longshore littoral drift (Michel and Howa, 1997, 2000), the choice of a 2DH model seems appropriate.

Some restrictions regarding the application of process-based models to long-term simulations need to be pointed out. Tidal parameters can be rigorously predicted, but the stochastic nature of storm occurrences makes wave-related parameters available only in statistical terms. Furthermore, the accurate modeling of wave propagation over a complex bathymetry remains a challenge, and the most advanced simulations still require extremely long computation times. These constraints define two possible approaches regarding the long-term morphodynamic modeling of a tidal inlet: a first approach consists of simulating separate events, i.e. representing the morphological changes induced by a series of typical storms alternating with calm periods. In order to be meaningful, such a model would have to be fully three-dimensional to correctly represent the action of waves on the sandbars. As far as we know, such simulations at the scale of an inlet and for the duration of a storm have not yet been carried out. A second approach consists in considering long-term evolutions by means of a process model run on time-averaged conditions, which is the method applied in this study.

A two-dimensional horizontal model was developed for this purpose, including a 2DH hydrodynamic module, as well as modules computing wave parameters, sediment transport and bathymetry updates. Sensitivity analyses were carried out to determine which tide and wave conditions were suitable for long-term simulations, as well as to optimize the required number of bathymetry updates and full hydrodynamic computations.

2. The Arcachon tidal inlet: geographical setting and morphological behavior

Unlike the rugged coasts of Brittany or the Atlantic coast of Spain, the French coast south of Bordeaux exhibits 250 km of straight sandy beaches, exposed to the rough climatic conditions of the Bay of Biscay. Several lagoons once interrupted this otherwise uniform coastline, of which the Arcachon lagoon is the only one still connected to the ocean through a morphologically active tidal inlet. The surface of the lagoon at high tide reaches 160 km^2 for a spring tide while at low tide, only the main channels remain passable, representing 40 km^2. The lagoon is separated from the ocean by an 18-km long sand spit, 1–5 km wide, made of aeolian dunes topping coarser marine sand (Fig. 1).

The inlet morphology can be separated into two major units: (1) the outer inlet, south of Cap Ferret (extremity of the sand spit), including a large ebb delta, made of major sand bars such as the Arguin and Toulinguet Banks through which the littoral drift bypasses the inlet; one or two alternately migrating channels are cut into the delta; (2) the inner inlet primarily consists of a small flood delta and a single channel following the east bank of the sand spit.

The tidal range varies between 0.80 m for neap tides and 4.60 m for spring tides, while winter storms on the Bay of Biscay induce a severe wave regime all along the Aquitaine coast. According to the classification of Hayes (1980), these features make Arcachon inlet a mixed energy tide-dominated inlet. The tidal prism for a mean spring tide was computed to be 347 Mm^3 in 1993 for a minimal cross-section of the inlet of 16 800 m^2.

While classical stability analyses lead to the classification of the Arcachon inlet as stable (Cayocca, 1996), its historical evolution exhibits cyclic trends typical of an ‘inherently unstable behavior’ (van de Kreeke, 1996). The morphological evolutions of the Cap Ferret sand spit were reconstituted from 1768 data (Gassiat, 1989). They exhibit two major phases of accretion (5 km from 1768 to 1826, including a progression speed of 185 m/year for 20 years, and 1894–1973), separated by a phase of retrogression (2 km). The position of the sand spit extremity was found to be related to the number and position of the inlet channels. Starting from a configuration with a single channel following the coast (called south channel, e.g. 1965, Fig. 2), a second channel (called north channel) opens up near the extremity of the sand spit (1826, 1905, 1987). This process parallels a retreat of the sand spit. Both channels progressively drift south and the north channel eventually merges with the south channel (1854, 1965). The resulting channel continues its drift southward while coming closer to the coast, eventually reaching La Salie (1923, 1990). The sand spit is stable or progrades during this phase. The north channel then opens up again. This behavior has been shown using bathymetric charts from 1826 until the present (Gassiat, 1989). Two cycles of approximately 80 years were identified. The amplitude and velocity of Cap Ferret morphological changes have significantly decreased in the past 25 years. However, the current evolution (i.e. deepening of the north channel, which is now used for navigation and erosion of the sand spit) confirms the cyclic behavior of the inlet.

3. Model outline and sub-model descriptions

Morphological evolutions are driven by nested processes that constantly interact: fluid flow, sediment transport and bathymetry are closely inter-dependent. Yet the evolution of the flow variables, and that of the seabed elevation occur at different time scales (Hauguel, 1978). This allows the decoupling of the hydrodynamic and bathymetric evolutions. Morphodynamic models thus do not need to solve coupled equations describing the simultaneous evolution of these linked parameters: the bed level is assumed to remain constant during the hydrodynamic computation while the flow and sediment transport are considered invariant during the bathymetry update (Wang et al., 1995). However, since waves and tidal currents are simultaneously taken into account, some nesting is required in order to represent the refraction of the waves by the tidal current and to compute the wave-induced current. This coupling will be described in Section 5.

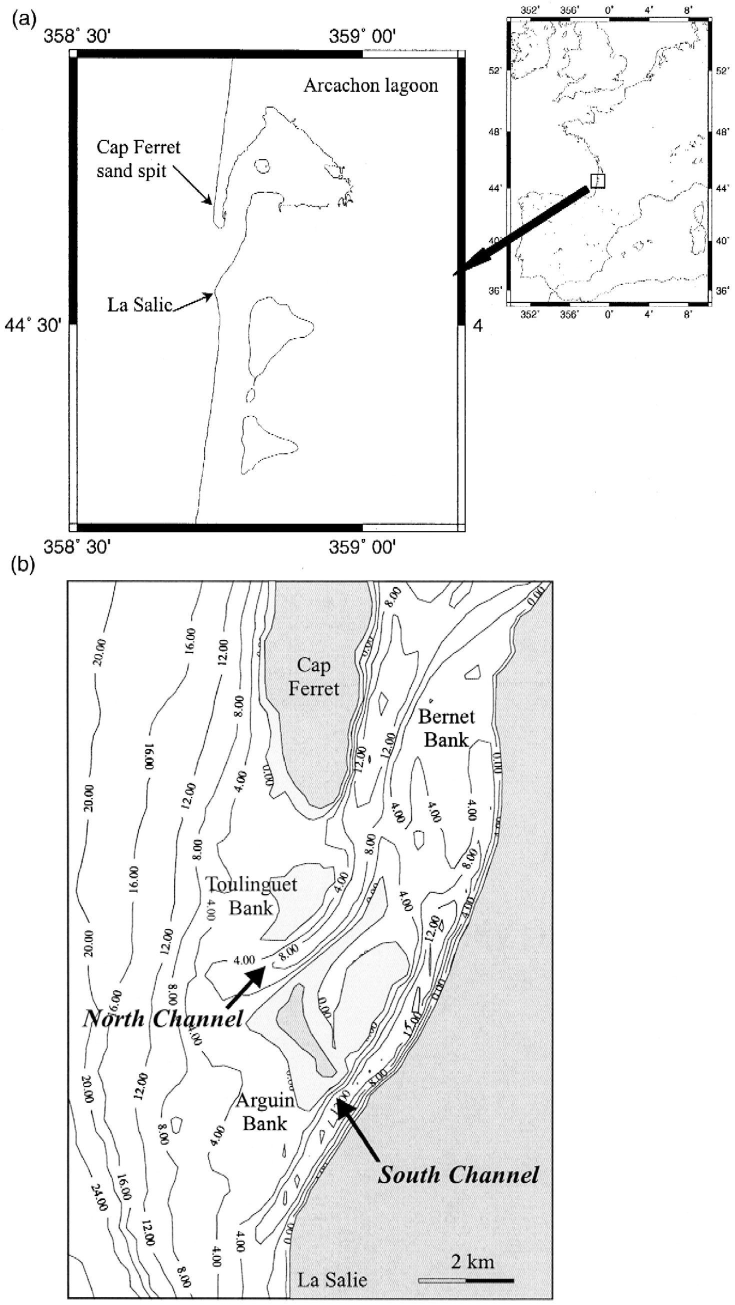

Fig. 1. (a) Location of the study area. (b) 1993 bathymetric chart of the inlet.

Long-term computations cannot take into account the most refined representation of all physical processes and input conditions. Each module, as well as the resulting nested model, are run under certain approximations regarding processes (which will be described for each individual module) and input parameterization (described in Section 4). Several techniques were also investigated in order to run the

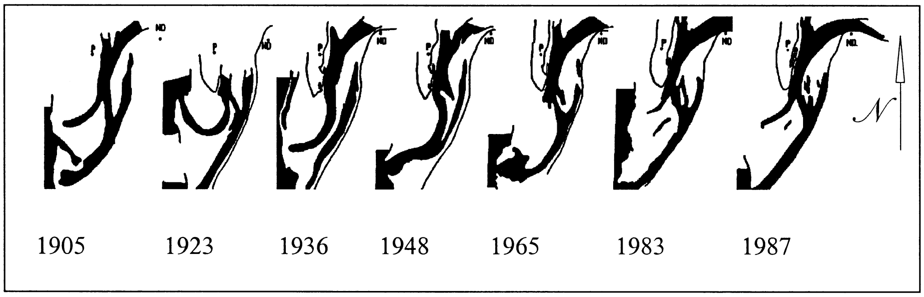

Fig. 2. Morphological evolution of the channels since 1905 (from Gassiat, 1989). The black areas represent water depths greater than 5 m.

model for longer periods of time without updating the bathymetry after each sedimentological time step or each tide (which would be extremely time consuming), and by avoiding a complete hydrodynamic computation after each bathymetric adjustment (Section 4).

The morphological model consists of:

- a wave module computing wave parameters for current and bottom shear stress calculations,
- a 2DH current module driven by tides and waves,
- a sediment transport module computing sediment fluxes,
- a bed-level module that updates the bathymetry in time,

described hereafter.

3.1. Wave module

The influence of waves is dominant along the Atlantic coast where it induces a net longshore littoral transport of 600 000 m^3 (Bellessort and Migniot, 1987). This transport is responsible for the constant southward drift of sand bodies across the inlet (Michel et al., 1995). Waves also play a determining role during storms by reshaping the sandbars of the ebb delta. We used the wave refraction model HISWA (Holthuijsen et al., 1989) to compute wave propagation across the domain. The model considers a steady state situation that requires the time of propagation of the waves through the domain to be short compared to the variation of other parameters (water level, currents, bathymetry). For the wave conditions used hereafter, the propagation time from the west side to the east side of the inlet is 15 min, which is short enough for the remaining parameters to be considered constant.

Diffraction is not taken into account by the model. Wave heights behind the sandbars are thus expected to be under-estimated. However, one of the main features characterizing wave propagation in the inlet is refraction by the currents which can increase the wave height by 50% (Bondzie and Panchang, 1993). Tidal currents are therefore taken into account in the wave computation (see Section 5). However, the two-dimensional structure of the model does not allow for the accurate representation of cross-shore morphological evolutions. Thus, the model will mainly represent morphological changes related to the longshore littoral transport.

Longuet-Higgins and Stewart (1964) showed that the driving forces of wave-induced current result from gradients in the wave-induced momentum flux. They derived an expression for the so-called radiation stress tensor as a function of the wave energy, the wavelength, the direction of propagation and the water depth. In the case of a shallow water approximation, the contribution of the waves to the Navier–Stokes equations integrated over depth reduces to the driving stresses F_x and F_y (Eq. 2) and to a modified bottom stress.

3.2. Current module

Currents are computed with a two-dimensional horizontal hydrodynamic model (Salomon and Breton, 1993) based on the shallow water equations:

$$\frac{\partial \zeta}{\partial t} + \frac{\partial (hU)}{\partial x} + \frac{\partial (hV)}{\partial y} = 0$$

$$\frac{\partial U}{\partial t}+U\frac{\partial U}{\partial x}+V\frac{\partial U}{\partial y}-fV=-g\frac{\partial \zeta}{\partial x}-\frac{1}{\rho}\frac{\partial p_{\mathrm{atm}}}{\partial x}-g\frac{\tau_{bx}}{\rho h}+\frac{F_x}{h}+\nu\left(\frac{\partial^2 U}{\partial x^2}+\frac{\partial^2 U}{\partial y^2}\right)$$

$$\frac{\partial V}{\partial t}+U\frac{\partial V}{\partial x}+V\frac{\partial V}{\partial y}+fU=-g\frac{\partial \zeta}{\partial y}-\frac{1}{\rho}\frac{\partial p_{\mathrm{atm}}}{\partial y}-g\frac{\tau_{by}}{\rho h}+\frac{F_y}{h}+\nu\left(\frac{\partial^2 V}{\partial x^2}+\frac{\partial^2 V}{\partial y^2}\right) \quad (1)$$

where

$$F_x=-\frac{1}{\rho}\left(\frac{\partial S_{xx}}{\partial x}+\frac{\partial S_{xy}}{\partial y}\right)$$

$$F_y=-\frac{1}{\rho}\left(\frac{\partial S_{xy}}{\partial x}+\frac{\partial S_{yy}}{\partial y}\right) \quad (2)$$

are the radiation stresses representing the contribution of waves.

The current velocities are vertically averaged, hence density currents and curvature-induced secondary flows are not taken into account. For sediment transport applications, the vertical velocity profile is assumed to be logarithmic in the direction of the flow. The computational grid is rectangular, with square meshes of 250 × 250 m. It includes the whole lagoon (160 km^2), and extends westward about 10 km offshore, 22 km north and 13 km south of the Cap Ferret. Boundary conditions are provided by a succession of two-dimensional models of decreasing sizes; the largest one covers the north Atlantic as far as 1°57′ west (offshore Spain), and includes the northern Spanish coast as well as the southern English coast along the English Channel. It is driven by the semi-diurnal tide M2. Water levels predicted by this model reproduce the measurements with an accuracy of 1 cm (Lazure and Salomon, 1991).

3.3. Bottom friction

Under the action of tides only, the bottom friction is expressed by means of a Strickler coefficient k_r:

$$\tau_{bx}=\rho g\frac{U\sqrt{U^2+V^2}}{k_r^2 h^{1/3}}$$

$$\tau_{by}=\rho g\frac{V\sqrt{U^2+V^2}}{k_r^2 h^{1/3}} \quad (3)$$

The non-linear enhancement of the bottom friction under the combined action of waves and current is represented by the model proposed by Soulsby et al. (1993). The authors define the mean velocity u_c of the flow resulting from the superposition of the tidal current and the waves; u_b is the amplitude of the orbital velocity of this flow. τ_c represents the shear stress associated with the velocity u_c if it resulted from tidal current only and is expressed as a function of the drag coefficient C_d (Eq. 4); τ_b represents the shear stress associated with the velocity u_b disregarding the presence of tidal current and is expressed as a function of the wave friction factor f_w (Eq. 5):

$$\tau_c=\rho C_D u_c^2 \quad \text{with} \quad C_D=\left(\frac{0.4}{\ln(h/z_0)-1}\right)^2 \quad (4)$$

$$\tau_w=\frac{1}{2}\rho f_w u_b^2 \quad \text{with} \quad f_w=1.39\left(\frac{a_0}{z_0}\right)^{-0.52} \quad (5)$$

The mean bottom friction τ_m resulting from the superposition of waves and currents, is directed against the direction of the mean current u_c:

$$\vec{\tau}_m=-\tau_m\frac{\vec{u}_c}{\|\vec{u}_c\|}$$

and is expressed by means of non-dimensional parameters x and y:

$$x=\frac{\tau_c}{\tau_c+\tau_w}, \quad y=\frac{\tau_m}{\tau_c+\tau_w} \quad (6)$$

related by the following expression

$$y=x\left[1+bx^p(1-x)^q\right] \quad (7)$$

where

$$b=\left(b_1+b_2|\cos\phi|^J\right)+\left(b_3+b_4|\cos\phi|^J\right)\log_{10}\left(\frac{f_w}{C_D}\right)$$

Table 1
Coefficient b, p and q as defined by Huynh-Thanh and Temperville (1991)

$b1$	$b2$	$b3$	$b4$	$p1$	$p2$	$p3$	$p4$	$q1$	$q2$	$q3$	$q4$	J
0.27	0.51	−0.10	−0.24	−0.75	0.13	0.12	0.02	0.89	0.40	0.50	−0.28	2.7

where p and q follow similar relationships (Table 1).

3.4. Sediment transport module

While sediment transport formulae including both bed- and suspended loads are commonly applied to morphological studies which consider the action of currents alone (de Vriend, 1994; Wang et al., 1995), the superposition of waves and currents makes the use of such formulae integrated over the wave period, a fairly crude approximation (Zyserman et al., 1991). However, the complete computation of suspended sediment profiles considering instantaneous values of wave and current parameters is far too costly to be applied to morphodynamic modeling. The principal processes to be represented by long-term models must therefore be identified in order to determine which case-dependant approximations can be made. Solutions described in the literature mainly include the use of two-dimensional horizontal flow models coupled with a local sediment transport formula (Watanabe, 1982; Ohnaka and Watanabe, 1990; Steijn and Hartsuiker, 1992), or a quasi-3D approach. The suspended transport is then computed assuming a logarithmic velocity profile and a concentration profile derived from the balance between turbulent mixing and gravity (Kamphuis, 1992; Briand and Kamphuis, 1993a,b; Wang, 1992; Wang et al., 1995). We considered the local formula of Bijker (1971) which computes separately the bed-load and the suspended load contributions.

The most frequent sediment grain size within the inlet corresponds to a medium beach sand. The model also covers the lagoon itself, where much finer sediments predominate. The morphological changes predicted by the model in the lagoon will therefore be inaccurate; in particular they are expected to be underestimated around the tidal flats. However, morphological changes inside the lagoon were shown to be quite minor compared to the evolution of the inlet itself: the comparison between bathymetric charts from 1865 and modern bathymetric data showed a simplification of the channel network inside the lagoon, with deepening of the main channels and accretion of the tidal flats (L'Yavanc, 1995). The tidal prism decreased slightly in the same time span (5%). These lagoon evolutions have not significantly affected the tidal current in the inlet itself. The inner lagoon morphology is therefore considered to be stable, and we will only use a single fraction of sand (350 μm).

The use of Bijker's formula results from the assumption that the suspended sediment load is a function of local conditions and is not connected to any upstream physical input. The computed potential transport is representative of the actual transport if a state of equilibrium with the flow conditions is reached. The fairly coarse fraction of sand considered here usually permits this approximation (Nicholson et al., 1997). However, the real sedimentological composition of the channels includes sand from 270 to 500 μm in diameter, as well as gravel and pebbles in certain areas (Bouchet, 1974). Outcropping layers of iron cemented sand stone were even observed in parts of the channels (Thauront, personal communication). The transport module will therefore overestimate the transport over a hard bottom or in areas covered with coarse sediments; it will also underestimate the transport of finer sediments, which is the common drawback of single grain size approximations. On the other hand, areas covered with gravel and pebbles correspond to areas flushed with the strongest currents, which explains why no fine sediments are found there. The strong currents will also give rise to the highest values of potential transport in areas where no more observed erosion takes place. To avoid artificial erosion in these areas of the model, they are represented by a non-erodible bed under a certain depth given by the initial bathymetry (where the hard bottom outcrops in the field). The sediment load is computed across

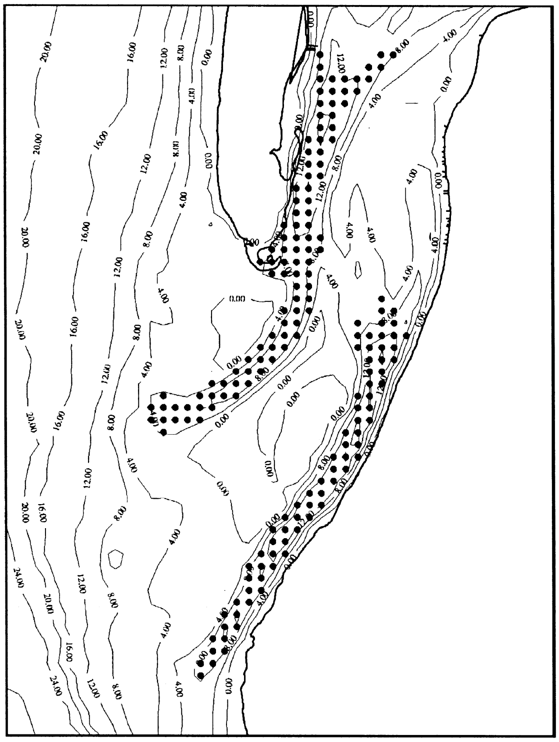

Fig. 3. The dots represent hard bottom where only deposition or erosion above the initial bathymetry is possible (area covered with pebbles or bedrock).

the whole domain and the deposition and subsequent erosion of sand originating from neighboring cells remain possible above the level of the non-erodible layer (Fig. 3).

The hydrodynamic time step Δt_h is 92 s in order to insure numerical stability. The sediment transport does not need to be computed as often. After a sensitivity analysis was carried out, the sedimentological time step Δt_s was increased to 552 s, i.e. the sediment load is computed every six hydrodynamic time steps:

$$Q(i\Delta t_s) = 6q\left(\vec{u}_{(6(i-1)+1)\Delta t_h}\right)$$

where Q is the sediment load over one sedimentological time step, and q is the sediment load computed over one hydrodynamic time step. The sediment fluxes integrated over one tide provide the net tidal sediment transport:

$$Q_{\mathrm{tide}} = \sum_{i=1}^{81} Q(i\Delta t_s)$$

3.5. Bathymetry update module

This module solves the equation for the conservation of sand:

$$(1-p)\frac{\partial h}{\partial t} - \frac{\partial q_x}{\partial x} - \frac{\partial q_y}{\partial y} = 0 \qquad (8)$$

where (q_x, q_y) is the sediment flux directed parallel to the velocity, i.e.

$$q_x = \frac{u}{u_{\mathrm{tot}}}q, \quad q_y = \frac{v}{u_{\mathrm{tot}}}q \qquad (9)$$

with

$$u_{\mathrm{tot}} = \sqrt{u^2 + v^2} \text{ and } q = q(u_{\mathrm{tot}}, h) \qquad (\mathrm{m}^2/\mathrm{s})$$

The system of equations to be solved when coupling the hydrodynamic, sediment transport and bathymetry update models is inherently unstable (de Vriend, 1987a,b); short-wave perturbations of the bed may therefore grow exponentially. This cannot be avoided by improving the numerical treatment of the equation since the instability arises from the differential equations themselves and not from their numerical implementation. This highly non-linear system may furthermore lead to unrealistic equilibrium profiles if slope effects — which occur in nature and tend to smooth the bathymetry — are not taken into account in the model (de Vriend et al., 1993a,b). Damgaard et al. (1995) describe several modes of slope related transport, among which downslope gravitational transport is the most commonly used in morphodynamic models (Watanabe et al., 1986; Maruyama and Takagi, 1988; de Vriend et al., 1993a,b). Following Hamm et al. (1994), we compared several methods to experimental results (Fredsoe, 1978) showing the evolution of the banks in a linear channel with an initially trapezoidal cross-section. After inspection, the transport was modified according to

$$\vec{q} = \vec{q}_0 + \varepsilon_s \|\vec{q}_0\| \vec{\nabla} h \qquad (10)$$

where q_0 is the transport computed on a flat bed and ε_s is an empirical factor weighting the influence of slope effects. Following Struiksma et al. (1985), we used $\varepsilon_s = 4$. The continuity equation thus becomes

$$(1-p)\frac{\partial h}{\partial t} - \frac{\partial}{\partial x}\left(q_x^0 + \varepsilon_s |q^0| \frac{\partial h}{\partial x}\right) - \frac{\partial}{\partial y}\left(q_y^0 + \varepsilon_s |q^0| \frac{\partial h}{\partial y}\right) = 0 \qquad (11)$$

de Vriend (1987a,b) used the characteristics analysis to investigate the interaction of currents and bottom evolution, for models consisting of a 2DH hydrodynamic model and a sediment model based on a local formula. The mathematical formulation of the system shows that the bottom evolution gives rise to a two-dimensional behavior of the bottom disturbances: a point disturbance will propagate in a triangular star-shaped pattern (just like a surface wave propagates in circles), while the convection part of the solution transports the disturbance in the flow direction. Several numerical schemes were used to account for the complex behavior of the system, use being made of a forward-time, central-space scheme with added numerical viscosity (Wang, 1991; Roelvink, in Nicholson et al., 1997), or of a Lax–Wendroff scheme (Andersen et al., 1991; Chesher et al., 1993; Tanguy et al., 1993). We tested two numerical schemes to solve Eq. (11), namely the Lax–Wendroff scheme as described by Chesher et al. (1993) and a forward-time, upwind scheme:

$$(1-p)\frac{h_{i,j}^{n+1} - h_{i,j}^{n}}{\Delta t} - k_1 \frac{q_{x,i+k_1,j}^{n} - q_{x,i,j}^{n}}{\Delta x} - k_2 \frac{q_{y,i,j}^{n} - q_{y,i,j+k_2}^{n}}{\Delta y} = 0 \qquad (12)$$

$$k_1 = (-1)\,\mathrm{sgn}(u)$$

$$k_2 = (-1)\,\mathrm{sgn}(v)$$

where n represents the time step and (i, j) the space coordinates; q_x and q_y are given by Eqs. (9) and (10). Both numerical schemes were applied to two simple cases: the one-dimensional propagation of a sinusoidal hump and the two-dimensional propagation of an initially sinusoidal dune in a rectangular channel subject to a steady current induced by a slope in the water surface elevation (Cayocca, 1996). The first test shows that gravitational slope transport was necessary to avoid a non-realistic steepening of the lee-side of the dune. For the second test (Fig. 4), both schemes show the progression of the dune in the direction of the flow, while the depth contours exhibit a triangular star shape expanding in all directions as shown by de Vriend (1987a,b). The height of the dune decreases with time, which is partly due to numerical diffusion, but also results from the nonlinear interactions between the current and bottom changes (de Vriend, 1987a,b). Both schemes provide similar results, although the forward-time upwind scheme is more diffusive and therefore gives rise to a smoother bathymetry. However, the morphodynamic model exhibited some instability when waves were added to the coupling of the hydrodynamic, sediment transport and bathymetry update sub-models, in which case the added diffusivity reduced these instabilities. While the Lax–Wendroff scheme is more accurate and did not generate instabilities under tidal forcing alone, we applied the forward-time upwind scheme to all simulations for consistency.

4. Long-term computation methods

Long-term morphological evolutions result from the succession of repetitive events such as tides and waves, with characteristic time scales varying from a few seconds to a few hours. Computations at the scale of several years or decades cannot take into account the real alternation of fortnightly tidal cycles. The ‘input filtering’ technique (as opposed to ‘process filtering’, de Vriend et al., 1993a,b) thus consists in defining representative tide (or wave) conditions with regard to sediment transport. In other words, the representative tide should induce the same sediment transport when repeated over a year as the real succession of spring and neap tides over the whole domain of interest. A unique representative tide does not necessarily exist; if not, it is usually possible to combine two ‘representative’ tides (Latteux, 1995). The influence of waves is more difficult to represent since their occurrence is not predictable, and their role on transport can only be assessed in terms of statistics. However, the yearly littoral transport may be taken as a reference; the representative wave conditions should therefore induce the same

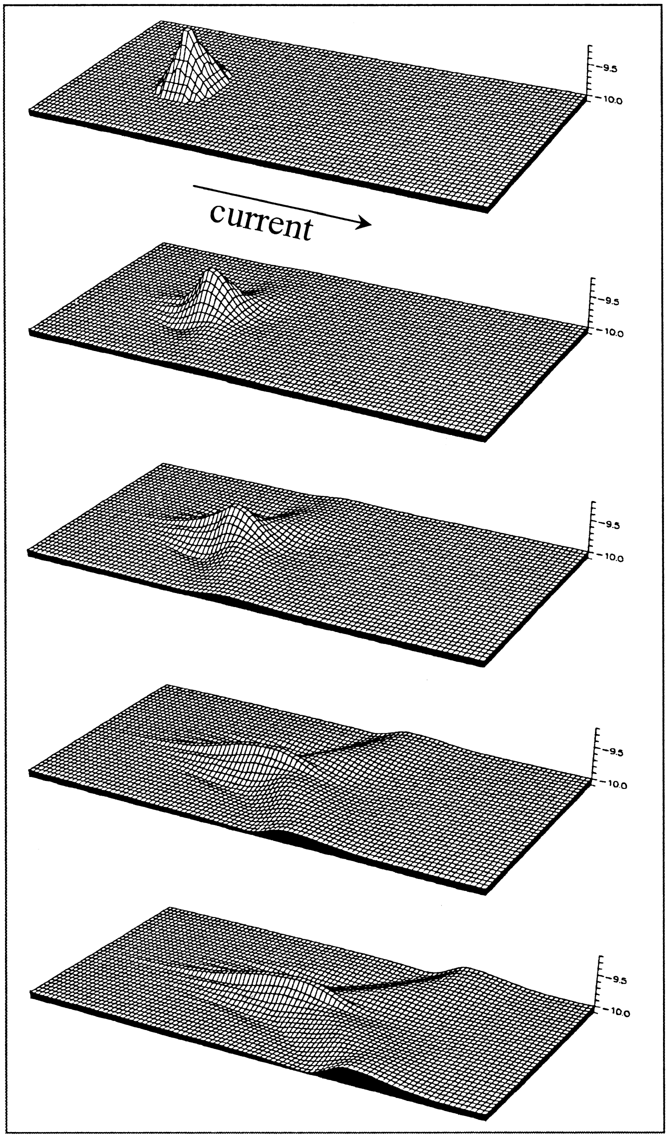

Fig. 4. Morphological evolution of a hump in a channel.

sediment transport over 1 year as do alternating fair and rough weather conditions.

4.1. Representative tide

A rigorous simulation of the sediment transport over several tides would require the complete computation of hydrodynamic conditions for each fortnightly cycle (this would actually be as rigorous as a sediment transport formula can be). Tides on the French Atlantic coast are dominated by the M2 component, and their amplitude is well represented by 'tidal coefficients' proportional to the semi-diurnal tidal range in Brest (Latteux, 1987). The 18.6-year periodicity of M2 tidal ranges may be used to compute a percentage of occurrence p_i of each tide T_i depending on its coefficient i (or tidal range, Gougenheim, 1953). The average transport field

φ_{mean} over one tide therefore reads for every grid point (x, y)

$$\varphi_{\mathrm{mean}}(x,y) = \sum_{i=\mathrm{coeff}} p_i \varphi_{T_i}(x,y) \tag{13}$$

where ϕ_{T_i} represents the transport field issued from the tide T_i. Both the direction and magnitude of the net transport over one tide vary depending on the tidal range. The representative tide T_{rep}, if it exists, is therefore defined as the tide that would result in a transport field uniformly proportional to the average transport, such as

$$\varphi_{\mathrm{mean}}(x,y) = \alpha\varphi_{T_{\mathrm{rep}}}(x,y) \tag{14}$$

for every (x, y), where α is constant across the whole domain. The average transport could therefore easily be deduced from the computation of this representative tide. Two methods proposed by Steijn (1992) and Latteux (1995) were investigated (Cayocca, 1996). Latteux's method allowed the definition of a single representative tide (mean spring tide), with $\alpha = 0.625$, i.e. it induces a transport which is 1.6 times as high as the mean annual transport everywhere, and in the same direction. The integrated sediment transport over a number n of tides will therefore be computed by running the model over $(0.625 \times n)$ representative tides. Inversely, for the morphodynamic model, the morphological changes found after running the model over n representative tides will correspond to the changes resulting from $(1.6 \times n)$ 'real' tides. This will have to be taken into account when running the model under combined tide and wave actions.

4.2. Representative wave conditions

The stochastic occurrence of storms or calm periods makes the representation of 'average' wave conditions extremely complex. Furthermore, the relationship between wave conditions and sediment transport is highly non-linear and depends on which physical processes are to be considered: while longshore sediment transport is proportional to $H^{5/2}$ (where H is the wave amplitude), the cross-shore transport is usually computed as a function of H^6 (Steijn, 1989). Depending on the type of transport to be modeled, the 'representative' wave conditions in regard to the transport will therefore be different.

Extreme storms may have drastic consequences on the beach morphology as well as on the configuration of the sandbars. Subsequent calm periods usually allow for replenishment of these areas, but some events may have irreversible consequences. However, long-term evolution of the tidal inlet (at the scale of decades or centuries) is strongly dependent on the global sediment input from longshore littoral transport. For instance, tidal inlet stability is shown to only depend on the littoral transport and on the tidal prism (which drives the tidal currents flushing the inlet, Bruun, 1986). Extreme events which shape the detailed layout of the inlet should therefore be modeled separately from the long-term trend (de Vriend et al., 1993a,b). They will actually require a much more accurate description of the physics involved. For long-term modeling purposes, we will therefore consider the longshore transport as the main process to be represented. This simplification is required in order to disregard complex interactions between various wave conditions superimposed on different tide conditions.

An average annual wave climate offshore of the Arcachon inlet was derived from three sets of data spanning 20 years (Table 2). Several formulae have been proposed in the literature to compute an estimate of the annual longshore sediment transport along a straight beach as a function of sediment related parameters, the beach slope and the wave conditions (height, period, angle of incidence; LCHF, 1973; Deigaard et al., 1986a,b; Kamphuis, 1991). When applied to the Arcachon schematic wave climate, they provide a value of 600 000 m^3 of net southward transport; this agrees with former estimates assessed from measurements (Orgeron, 1974). The schematic wave climate will therefore be used to determine a set of representative conditions.

Table 2
Simplified annual wave climate at Arcachon

	H_s (m)	T (s)	p (%)
Type 1	< 0.5	6	20
Type 2	1	8	50
Type 3	2	11	20
Type 4	3	13	8
Type 5	5	17	2

Two methods of wave schematization proposed by Steijn (1992) and Chesher and Miles (1992) were compared (Cayocca, 1996). They consist in selecting a few schematization points in shallow water areas where wave parameters (height, period and angle of incidence) are computed with a one-dimensional wave model for each condition of the wave climate. A set of transport related parameters and associated weighting factors is computed at each point and is used to determine one or several representative wave conditions depending on how widely the angles of incidence are spread. The interaction between waves and tidal currents or variations of the water level during one tide are not taken into account. The schematization points were thus chosen where tidal currents can be disregarded, i.e. outside the inlet. This strategy is consistent with the idea of finding wave conditions representative of the longshore littoral transport. Since the wave climate in Arcachon is strongly dominated by waves coming from the north-northwest, it was possible to find a unique set of representative conditions.

The longshore littoral transport computed with both sets of representative conditions was compared to the measured value of 600 000 m^3. Chesher and Miles' method leads to a slightly underestimated result compared to Steijn's method. The latter allowed us to determine a unique set of representative conditions: significant wave height $H_s = 1.80$ m, wave period $T = 9$ s, angle of incidence $\alpha = -22.5°$ (i.e. NNW), percentage of contribution $p = 75\%$ (i.e. frequency of occurrence of the representative waves).

4.3. Stretching of the morphological time step

Several time scales characterize the morphological model:

- The hydrodynamic time step Δt_h is the time step of the current model. It was set to 92 s to insure stability. Each tide therefore requires 486 hydrodynamic computations.
- The sedimentological time step Δt_s is the time step between sediment transport computations (for initial transport calculations). Here $\Delta t_s = 6\Delta t_h$, i.e. each tide requires 81 sediment transport computations.
- The tidal period T (44 712 s ≈ 12 h 25 mn).
- The morphological time step ΔT_m represents the time required for the bottom change to be significant enough to justify an update of the bathymetry. It is related to the morphological tide, which represents a number N of real tides. Complete hydrodynamic computations may or may not be carried out at each increment of ΔT_m: if the evolution of the bathymetry is small enough, the flow parameters may be adjusted by continuity without making the complete hydrodynamic calculation. In that case, a full hydrodynamic computation is carried out every $(M+1)(\Delta T_m)$ where M is the number of adjustments by continuity. This adjustment rests on the hypothesis that the flow pattern and local discharge magnitude remain unchanged through the bathymetry update (Hauguel, 1978; Wang, 1991; Latteux, 1995; Ribberink et al. 1995). For two-dimensional flows, this approximation is only valid for small variations of the seafloor, after which an entire hydrodynamic computation has to be carried out. We will investigate the validity of this approach next.
- The wave computation time step ΔT_w represents the number NH of morphological tides after which complete wave and hydrodynamic computations have to be carried out ($\Delta T_w = \mathrm{NH} \times N \times T$).

Bathymetric evolutions resulting from one tide are negligible. One solution to avoid updating the bathymetry after each tide is to stretch out the morphological time step. Two methods proposed by Latteux (1987, 1995) were investigated along with an adjustment of the flow parameters by continuity in order to similarly reduce the number of hydrodynamic computations. 'Centered extrapolation' is a trial and error method. It considers that the flow is not affected by the bottom evolution under a certain threshold ε of the relative bottom change $\Delta h/h$. The bottom change over the first tide, Δh_1, is computed over the entire domain and is then extrapolated over N tides, N being the largest integer satisfying

$$\max_{\text{domain}}\left(\frac{N\Delta h_1}{h}\right) \le \varepsilon \tag{15}$$

The bathymetry is then updated according to the first tide bottom change (h becomes $h + N\Delta h_1$), and the bottom change over the tide $N+1$ is computed

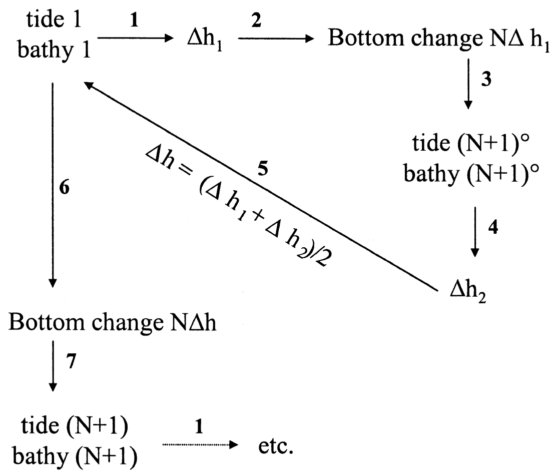

Fig. 5. Principle of the centered extrapolation method.

(Δh_2). The bottom change to be applied over the N first tides becomes $N(\Delta h_1 + \Delta h_2)/2$ (Fig. 5). The currents and water elevations are then updated either by continuity alone or by running the hydrodynamic model with the new bathymetry.

The 'tide stretching' method consists in representing N successive tides by a single tide, which is equivalent to juxtaposing identical phases of successive tides (Fig. 6). The morphological time step therefore equals N times the sedimentological time step. The bathymetry is updated after each morphological time step. This method does not allow adjustment of the flow properties by continuity, since the tide conditions change from one morphological time step to the next. Fig. 7 shows the time stepping procedure for both methods.

Sensitivity analyses were carried out for both methods to determine the maximum values of N and M by comparing the results to a reference simulation which updates the bathymetry after each sedimentological time step during 10 tides (Cayocca, 1996). For the centered extrapolation method, it was shown that N cannot exceed 20 without inducing noticeable discrepancies. The number of continuity adjustments tends to cancel out these discrepancies; however, for large values of M the approximation of the conservation of fluxes is no longer valid. After the third continuity adjustment (for $M > 3$), the current modifications are underestimated, as is the morphological evolution. The optimum values of the driving parameters for the centered extrapolation method were therefore set to $N = 20$ and $M = 3$. For the tide

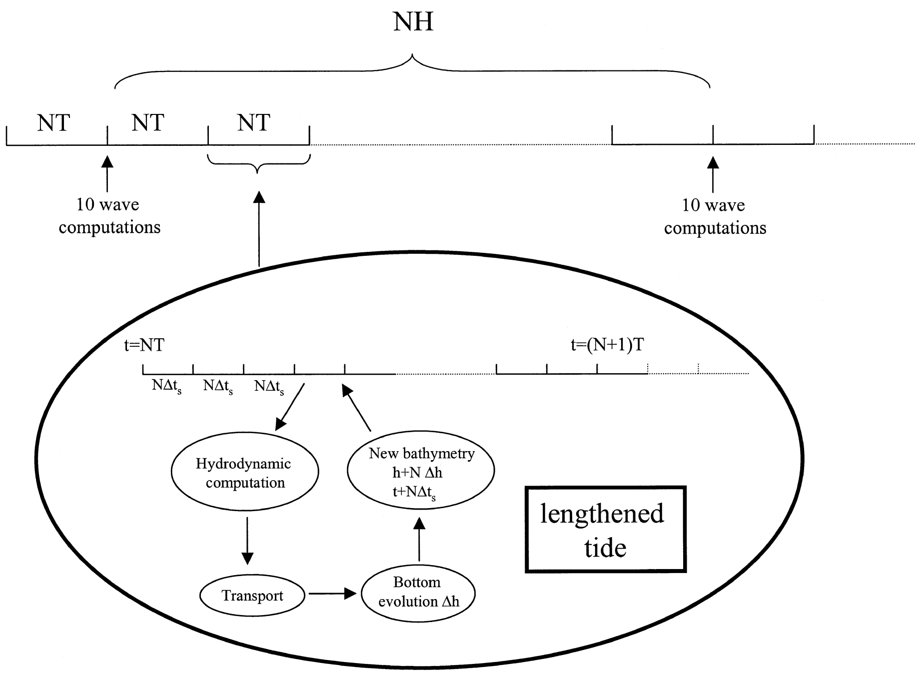

Fig. 6. Principle of the lengthened tide method.

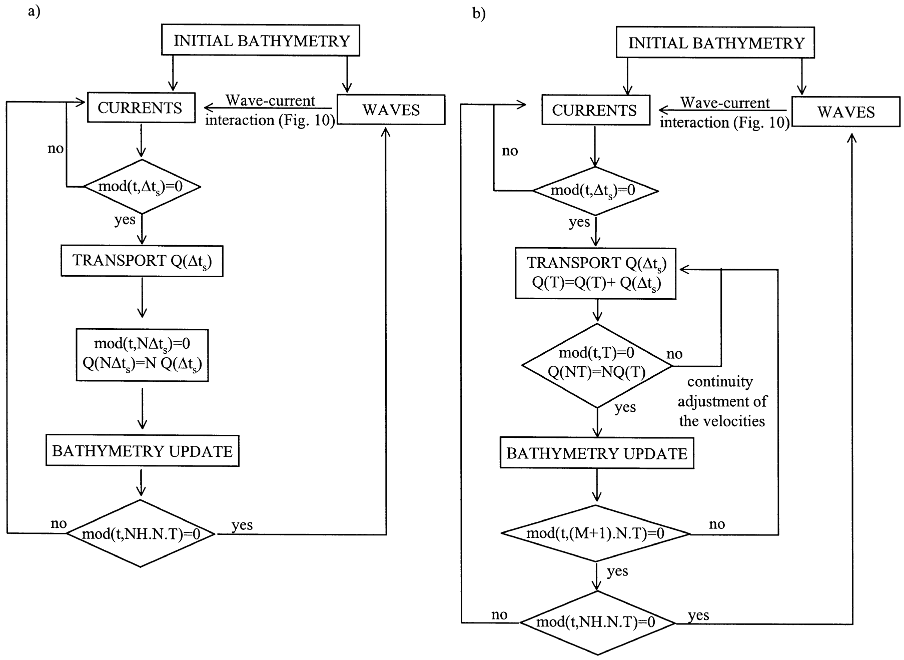

Fig. 7. Time stepping procedure for: (a) the extrapolation method and (b) the lengthened tide method.

stretching method, the bottom changes are well represented for values as high as $N = 30$, after which some discrepancies are observed.

In order to determine which method induces the least amount of errors, we compared the results of both methods for $N = 10$ to the reference simulation (Fig. 8a). The centered extrapolation method creates a morphological evolution that diverges from the reference simulation (creation of a 'fork' in the newly opened channel, which does not appear in the reference simulation). Increasing values of M smooth the morphological changes but do not eliminate this fork, which does not appear when the lengthened tide is used. This is probably due to the fact that the continuity adjustment allows the propagation of the bed-forms without taking into account the processes responsible for their growth. The stretched tide method was therefore chosen with $N = 30$, which does not induce significant discrepancies compared to $N = 10$ (Fig. 8b).

The rate of bathymetric changes does not justify the complete computation of wave parameters after each update of the bathymetry. We investigated the optimum value of the number of morphological tides NH after which the wave model had to be run again. The reference simulation ran wave computations every five morphological tides. Morphological changes after five morphological tides are moderate enough to justify this approximation. Fig. 9 displays the morphological evolutions for NH = 20 as a function of the evolutions for NH = 5 after 30 and 75 morphological time steps, respectively. Discrepancies increase with time in both number and amplitude; however, the errors induced for NH = 20 do not affect the general shape of the bars and channels (they mostly occur at singular points, due to local irregularities of the wave module output), and were considered acceptable. It should be mentioned that the value of NH closely depends on the value of N: for a shorter morphological time step, bottom evolutions after each morphological tide would be smaller, allowing for greater values of NH.

5. Model implementation

Fig. 7a shows the time-stepping procedure that was applied for the simulations presented in this paper (with $N = 30$ and NH = 20). Modeling of the

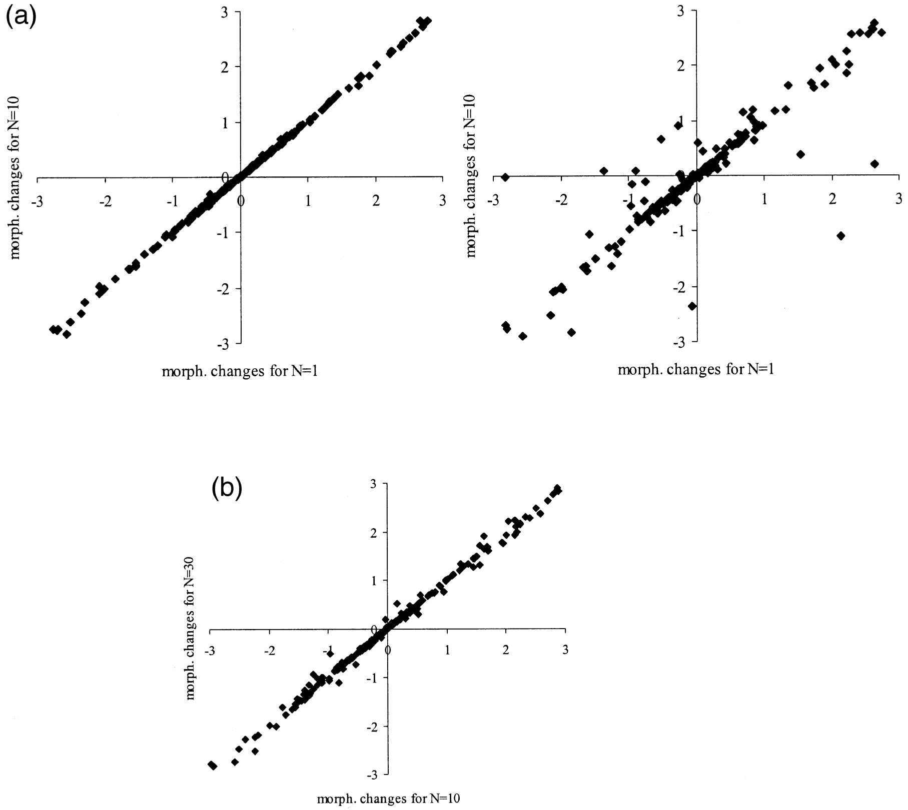

Fig. 8. (a) Amplitude of the morphological evolution (in m) over 10 representative tides vs. the amplitude of the evolutions over one tide. Left: for the lengthened tide with $N = 10$; Right: for the centered extrapolated method with $N = 10$ and $M = 0$. (b) Amplitude of the morphological evolutions (in m) over 30 representative tides vs. the amplitude of the evolutions over 10 tides for the lengthened tide.

interaction between waves and current remains to be described: wave propagation is affected by both water depth and refraction by the currents, while waves induce a current themselves when reaching shallower

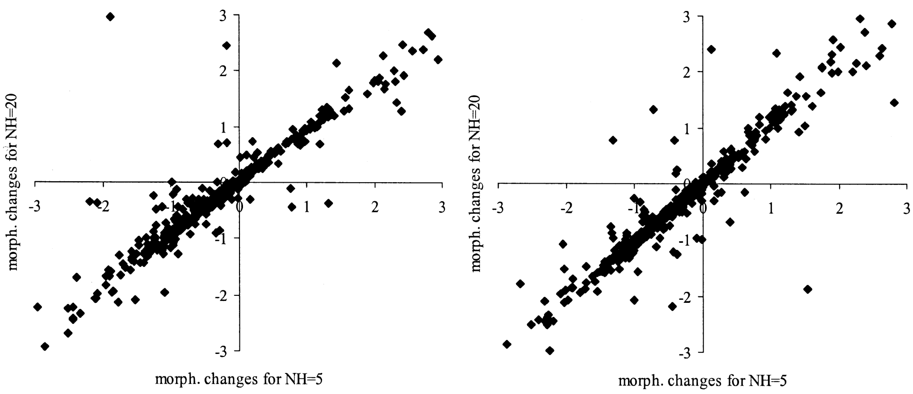

Fig. 9. Amplitude of the morphological evolutions (in meters) for NH = 20 vs. the amplitude of the evolutions for NH = 5 after 30 (left) and 75 (right) morphological time steps.

water. When waves are introduced in the model for the first time, these interactions have to be taken into account by running alternately the current and wave modules. The main outputs of the wave module used for sediment transport computations are the orbital velocities and the modification of the tidal current, both of which depend on the phase of the tide. The propagation time of the representative waves across the tidal inlet is 15 min, which is therefore the minimum amount of time between two consecutive wave computations. Water elevation and intensity of the tidal current exhibit a relative phase shift of $\pi/2$, i.e. water levels vary the most at extrema of the current velocity and the current gradient is at a maximum for high and low tides. Since both current and water level influence the propagation of the waves, a sensitivity analysis was carried out to determine the most proper discretization in time: were the wave driven currents best reproduced if the computations were spaced at regular intervals of the water level or at regular intervals of the current velocity? Ten computations per tide were carried out for each discretization. Comparison with a reference computation running the wave model 27 times per tide (i.e. every 27 min) showed that computations at regular water level intervals gave the best results (Cayocca, 1996).

The hydrodynamic parameters of the first tide are stored for the 10 relevant time steps, and used as an input for 10 wave computations. Resulting radiation stresses and orbital velocities (used for the bottom shear stress computation) are in turn injected into the hydrodynamic model where they are considered constant during a time period centered on the time of wave computation (Fig. 10). The currents resulting from this first iteration can be stored for possible further iterations. However, it was shown that a second computation of the radiation stresses and orbital velocities taking into account refraction by the new currents does not significantly affect the results of a third hydrodynamic run. Furthermore, during a full run of the morphodynamic model, wave computations carried out after a bathymetry update will take into account former tide and wave induced currents. The hydrodynamic module will therefore be run twice at the first introduction of waves, and only once after each new run of the wave model.

Representative tide and wave conditions were separately defined with regard to sediment transport. The interaction between tidal currents and waves is non-linear; the linear superposition of these conditions assessed independently might therefore seem questionable. However, areas where waves or tidal currents dominate are geographically disjointed. Most

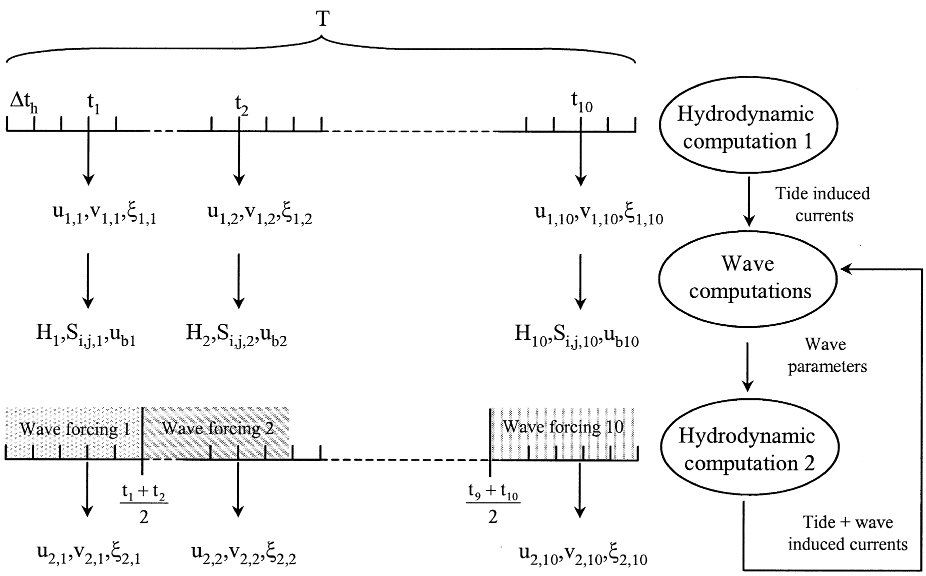

Fig. 10. Coupling between tide and wave forcings for hydrodynamic and wave computations.

waves break on the ebb delta sandbars, which reduces in a large extent wave action within the inlet: the wave height inside the inlet reaches 0.6 m for 6-m waves offshore (Gassiat, 1989). Tidal currents therefore strongly dominate longshore sediment transport in the tidal inlet while their influence is negligible along the coast north and south of the inlet. The maximum tidal current velocity along the coast reaches 0.15 m/s for a spring tide, while the wave-induced longshore current reaches 0.80 m/s for a 2 m wave height (fair weather) and 1.45 m/s for 6 m wave heights (LCHF, 1969). The representative tide aims at reproducing the mean transport within the inlet while the representative waves aim at reproducing the mean littoral transport along the coast and on the offshore side of the ebb delta.

The previously defined representative wave conditions turned out to have very little effect on the morphologic evolution of the inlet as compared to the simulation with no waves, particularly with regard to the southern drift of sandbars reported in the literature. The following factors can explain this result.

(1) The representative tide induces a transport 1.6 times greater than the 'actual' tidal transport computed over a year: this discrepancy could be reduced by finding representative wave conditions inducing 1.6 times the observed longshore littoral transport.

(2) We considered a uniform grain size across the whole domain. Sand offshore the ebb delta happens to be finer than in the channels (Bouchet, 1974), in which case the same current would induce more transport along the beaches of the sand spit than in the inlet. Even if the magnitude of the littoral current is well reproduced by the representative wave conditions, the computed transport inside the inlet will be underestimated because of the locally coarser grain size.

(3) The representative wave conditions were designed to give a good estimate of the longshore drift along the coast. These conditions are considered 'fair weather conditions' in this area where waves less than 1 m are exceptional. The 1.80-m representative waves break on the beach along the straight coastline and on the shoals of the outer ebb delta during the ebb. They propagate beyond the sandbars of the outer delta during the flood without exceeding 1.30 m in height. Storm waves induce a different pattern: they break further offshore and must induce a strong transport around the outer delta, both cross-shore and longshore. Storms are therefore responsible for a 'bulldozer effect' (de Vriend and Ribberink, 1993), preventing the tidal delta from extending further seawards (an extension which is visible in the simulations without waves). Therefore, neglecting the cross-shore transport in our computations turns out to be an invalid approximation even for the study of long-term trends. Subsequent computations were carried out with more severe wave conditions allowing a better representation of the storm-induced bathymetric changes.

There are no measurements of the cross-shore transport in the area. Considering that the cross-shore transport is proportional to H^6 (Steijn, 1992) and results from the contributions of each category of waves encountered throughout the year, we used wave height statistics (Orgeron, 1974) to compute a new 'representative' height H_{CS} according to

$$H_{CS} = \left(\sum_i p_i H_i^6 \right)^{1/6}$$

where p_i is the probability of occurrence of the wave height H_i. We found $H_{CS} = 4$ m, and used a corresponding period of 13 s (which is the most frequent period measured for that wave height), and the same direction of propagation as before, i.e. north–northwest (the dominating direction for storms). This new definition of a wave regime to be applied to further computations is a somewhat cruder approximation of representative wave conditions than previously described. However, since cross-shore transport generated by undertow is not properly taken into account by the vertically averaged scheme, refinement in describing representative wave conditions regarding cross-shore transport seems unwarranted.

6. Results

6.1. Tidal forcing alone

Fig. 11 shows the instantaneous transport field at the maximum intensity of flood and ebb for the representative tide, as well as the residual tidal transport. Most of the inlet is dominated by the ebb

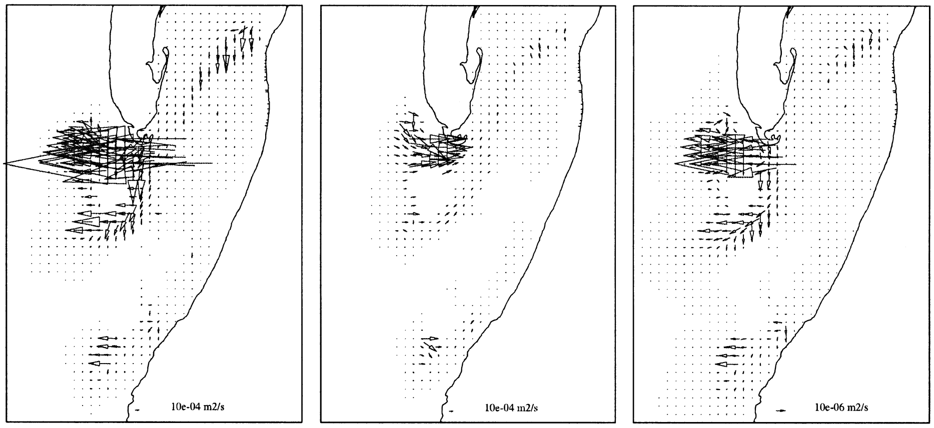

Fig. 11. Computed sediment transport field for a mean spring tide: maximum ebb transport (left), maximum flood transport (center) and residual tidal transport (right). Current velocity reaches 2 m/s near the extremity of the sand spit while it is only 20 cm/s in the inner inlet, which explains the large magnitude of the transport South of Cap Ferret.

transport, except in the northeast where the flood dominance explains the development of the Bernet Bank. The southern channel exhibits almost no net transport and most morphological changes would be expected for the sand spit extremity as well as for the northern channel (as long as the bottom sediment allows for erosion).

Fig. 12 displays the result of the simulation of 150 morphological time steps, i.e. 4500 representative tides. Since most of the northern channel is covered with pebbles, the most active area is located at the extremity of the sand spit where the initial embryonic channel is quickly deepened while levees are built along both sides. The orientation of this channel shifts from the west to the northwest, and the southern sandbars of the inlet widen.

The Cap Ferret southern flank steepens, which does not conform to observations reporting a severe erosion of the spit which tends to recede. The maximum slope computed after this simulation does not reach the value of the maximum slope measured on the initial bathymetry; the use of a maximum slope criterion thus would not allow the correct representation of the spit's retreat. The fairly large size of the grid cells (250 m) induces an artificial smoothness in the bathymetry, which explains why the introduction of a transverse component of the transport to represent curvature effects does not improve the results.

Recalling that the residual transport induced by a representative tide over 1 year is 1.6 times higher than the mean annual transport, the 150 morphological time steps span about 10 years. According to historical records, the opening of a 'functional' channel (i.e. deeper than 5 m) takes 10–20 years (1896–1905, 1965–1987, see Fig. 2). This simulation shows the opening of a functional channel after 20 morphological time steps, i.e. 16 months. Several reasons may explain this discrepancy.

In the absence of waves, no process prevents the tidal ebb delta from extending seawards as it does under tidal forcing alone. The main action of the tidal currents is to flush the inlet through existing channels. The simulation does not include any process that might induce the breaching of existing sandbars. Since ebb currents are stronger than flood currents in most of the inlet, the model predicts the transport of the sediments toward the ebb delta, as long as there is available sediment.

The use of a uniform grain size in the model probably leads to an overestimate of the transport through the inlet: the presence of shell debris (Orgeron, 1974) and coarse sediments in certain areas necessarily limits the actual transport. Furthermore, the degree of accuracy of sediment transport formulae in the ocean has been proved to be fairly low (Soulsby, 1995), and no transport measurements have been carried out in the Arcachon inlet for comparisons.

The longshore littoral transport induced by the waves is disregarded. The continuous sediment input

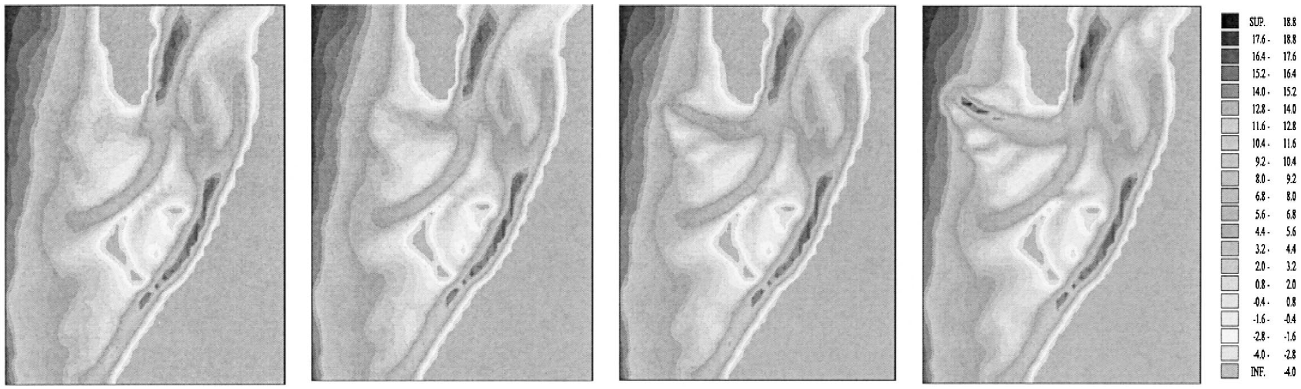

Fig. 12. Initial 1993 configuration and simulated morphological evolutions after 10, 50 and 150 morphological time steps (tide only).

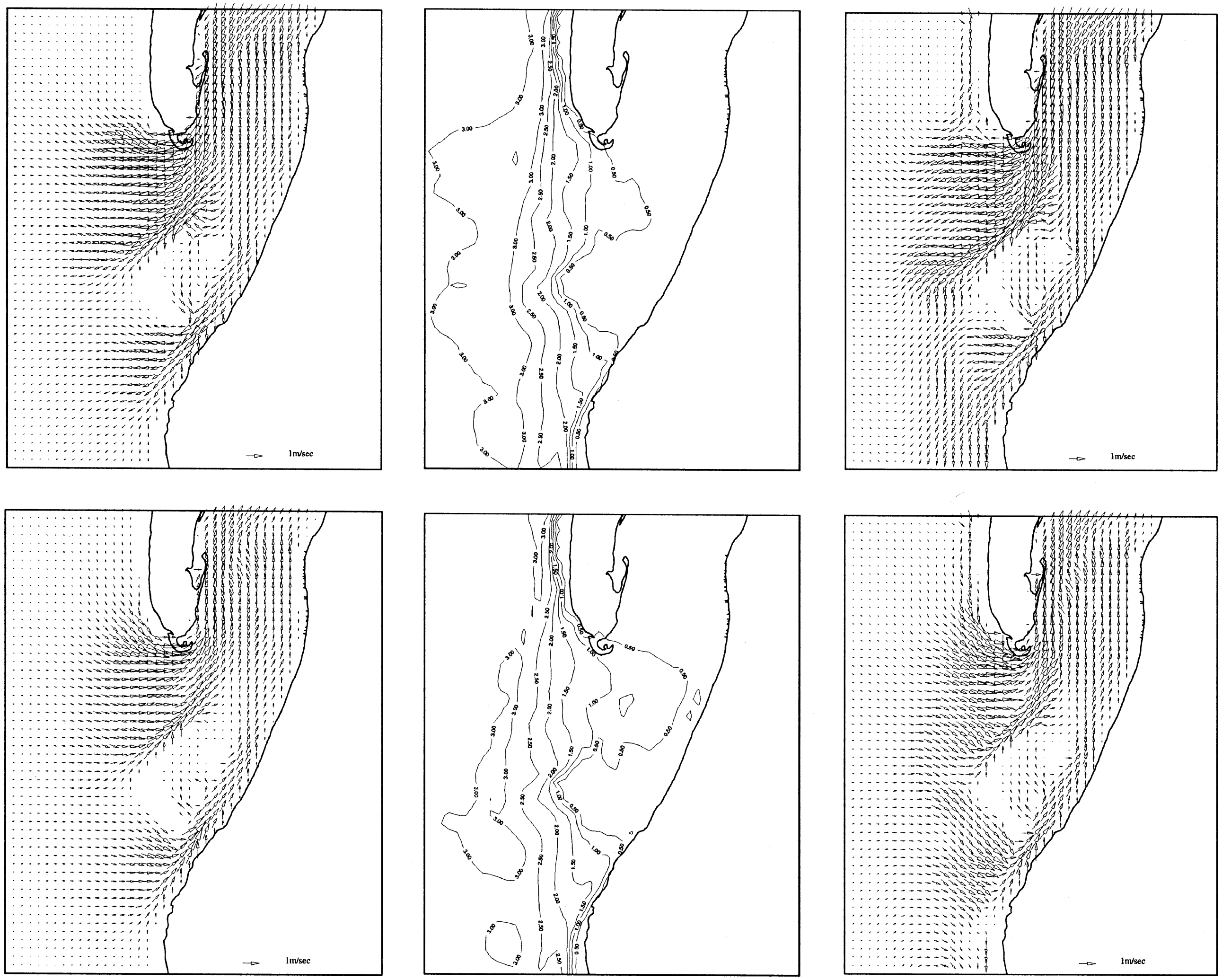

Fig. 13. Top: tidal flood current (left); computed wave heights including refraction effects (center); flood current resulting from the superposition of tide and wave effects (right). Bottom: idem for ebb current.

to the inlet being interrupted, the creation of smooth deep channels is not surprising. Eventhough sediment issuing from longshore transport mostly bypasses the inlet (Michel and Howa, 1997), it somehow reshapes the inlet's configuration.

These observations stress the difficulty of calibrating simulations in a complex situation where many physical processes would have to be taken into account for sounder results. However, this first simulation emphasizes the role of the tide in opening new channels, while showing that wave forcing has to be taken into account for more realistic simulations.

6.2. Tide and wave forcing

Fig. 13 shows the influence of waves on the tidal currents for the flood and ebb. Waves do not affect the currents inside the tidal inlet north of the Cap Ferret. Their influence is particularly noticeable in the outer inlet at low tide and high tide, when the longshore littoral current is the most visible. The wave contribution does not stand out as much when superimposed on ebb or flood currents. However, it increases the southern component of the current velocities and strengthens the flood currents at the extremity of the sand spit. The asymmetry between flood and ebb currents is well reflected by the transport since the ebb transport can be five times greater than the flood transport (magnitude of 10^{-4}–10^{-5} m^2/s). The residual tidal transport is therefore strongly dominated by the ebb, particularly within the offshore extremities of the channels, while the effects of the southern drift are seen across the whole inlet (Fig. 14). The eastward component of the residual transport at the extremity of the sand spit is increased, which should slow down the creation of a northern channel as simulated in previous runs.

Fig. 15 displays the morphological evolution of the 1993 bathymetry under combined tide and wave actions. Numerical irregularities are responsible for a number of non-significant features (mainly due to divergences of the wave module run over a rough bathymetry). Our goal here is therefore to concentrate on the most representative features resulting from the introduction of waves: a channel is dug at the extremity of the sand spit as was the case in the previous simulation. The general deepening of all channels is compensated by the nourishment of the existing sandbars while small 'islets' separate and drift south.

Since we attributed the irregularities of this simulation to the complexity of the bathymetry, we ran the model on a hypothetical configuration where the inlet bottom is set to a uniform depth of 3 m. The

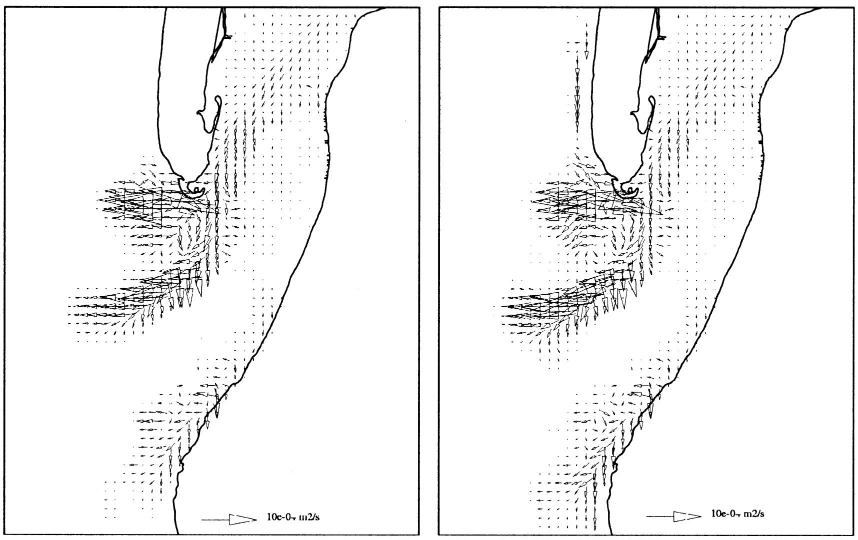

Fig. 14. Residual transport over the representative tide without (left) and with (right) waves (logarithmic scale, the reference arrow represents 10^{-4} m^2/s).

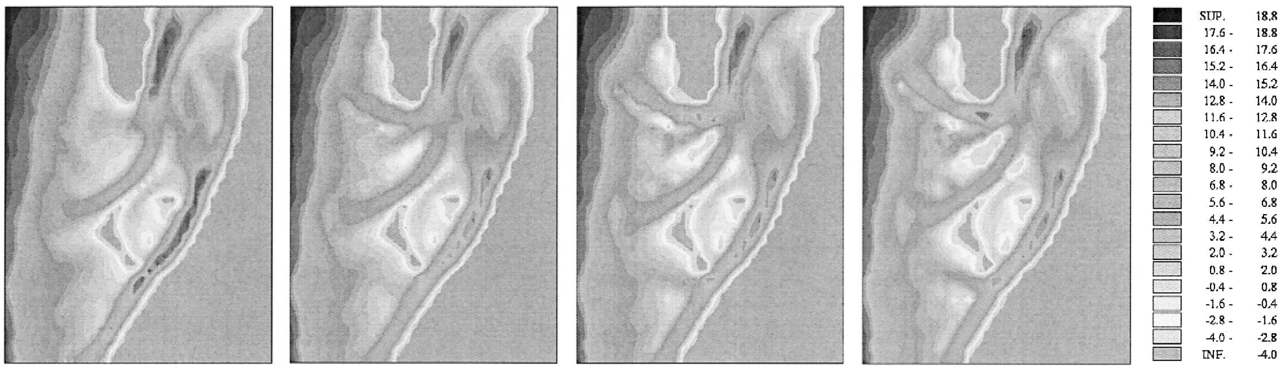

Fig. 15. Initial 1993 configuration and simulated morphological evolutions after 20, 50 and 80 morphological time steps (tide and waves).

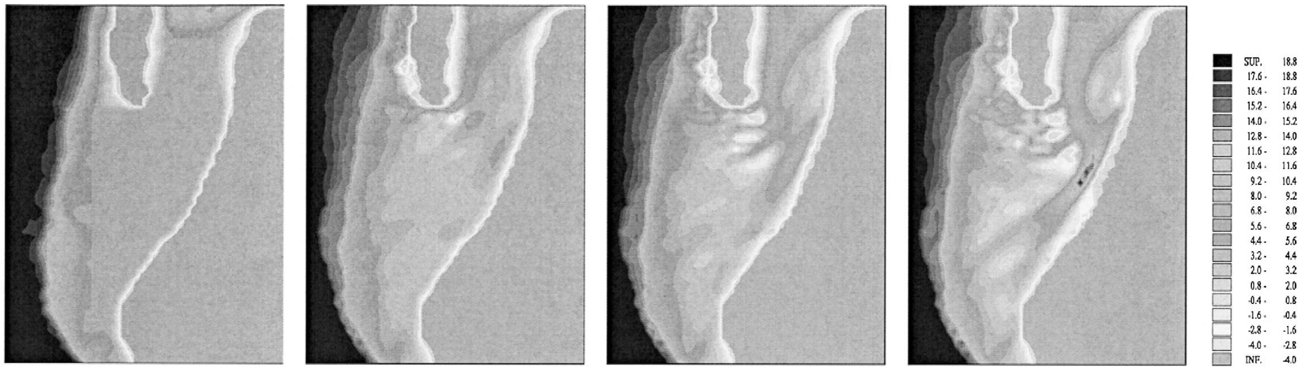

Fig. 16. Initial flat configuration and morphological evolutions after 50, 100 and 150 morphological time steps (tide and waves).

resulting bathymetry after 180 morphological time steps exhibits several features which show a remarkable resemblance to either present or past situations (Fig. 16). The most striking one is the opening of a main channel along the southern coast (a single channel configuration was observed around 1900 and again around 1965). The flood domination of the residual transport east of Cap Ferret builds up a sandbar comparable to the present Bernet Bank. The main channel is limited to the west by a large sandbar migrating to the south (recalling the modern Arguin Bank), at the extremity of which smaller units separate to meet with the coast at La Salie, in accordance with historical observations (Michel et al., 1995). The southern extremity of the sand spit is blocked by little sandbars built up by the waves (Fig. 16) which prevents the opening of a northern channel as shown in the simulation without waves.

7. Discussion

The main purpose of this work was to investigate the possibility of reproducing long-term trends in the morphological evolution of a tidal inlet, using a 2DH process model driven by a steady forcing. The complex bathymetry of the lagoon and its interaction with the inlet impose its entire inclusion in the computational domain in order to insure a good representation of the tidal currents in the inlet (Salomon, 1995, personal communication). The 2DH hydrodynamic model was shown to provide accurate flow velocities (Salomon and Breton, 1993). The two-dimensional approach can be a severe restriction when waves and currents interact, particularly around tidal inlets, because of the interaction of the tidal current with other coastal currents (van de Kreeke, 1996; Ranasinghe et al., 1999). However, we made the assumption that long-term evolutions were mostly driven by longshore currents (as opposed to cross-shore currents), in which case a three-dimensional approach was not as essential. It is nonetheless an approximation, which makes the extreme refinement of other processes pointless.

The complex behavior of tidal inlets and the interactions between several processes make the validation of morphodynamic models with data difficult. Eventhough each sub-model may have been separately tested, their combination forms a new system which may not provide convincing results (de Vriend et al., 1993a,b). Capacities and limitations of morphodynamic models can be investigated on simple theoretical cases where all parameters can be clearly identified (e.g. Nicholson et al., 1997). Another option consists in applying these models to real cases where abundant data is available, such as areas where human interference has provided well documented forcing and monitoring. This was not the case for the Arcachon inlet where the strength of natural processes has heretofore hindered significant human intervention. However, comparison with past evolutions points out the limitations of the model, which reflect the approximations that were made:

The two-dimensional scheme does not allow for an accounting of the vertical profile of the velocities, which can lead to spurious results when undertow, wave asymmetry, bottom boundary drift or curvature-induced secondary flows cannot be ignored. Eventhough the magnitude of these processes might be small, their final effect on the residual transport can be significant (Wang et al., 1991). In the case of the Arcachon inlet, secondary flows might be responsible for channel migration while wave-related cross-shore transport has a dominant effect within the surf zone of the outer delta. Although longshore transport is thought to be dominant for the long-term evolution of the inlet, cross-shore processes drive the short-term morphological changes during storms. The apparent cyclic nature of the configuration of channels is a long-term feature; however, it cannot be reproduced without taking into account short-term events (such as the opening of a breach during a storm).

Local sediment transport formulae provide a poor approximation of true transport, particularly under the influence of combined waves and currents and on highly uneven bottoms (Komar, 1996; van de Kreeke, 1996). When integrated into a morphodynamic model, this factor has dramatic consequences, since different formulae may lead to very different patterns of evolution in the long-term (Cayocca, 1996). If a three-dimensional approach is chosen, vertical diffusion and advection can be accounted for. However, an accurate modeling of transport in the swash zone will be extremely costly. The approximation of a single fraction of sediments can also lead to under-or overestimates of the actual transport, which is the case in the Arcachon inlet where shell debris and sand stone layers have been reported.

The 250×250 m grid size affects the quality of the results, particularly around the extremity of the sand spit and in the inlet where the channel width does not exceed 2–4 cells. This fairly coarse resolution also affects the representation of the waves, especially in the surf zone: the littoral drift is known to be limited to a 500-m wide littoral strip, which corresponds to only two cells. Moreover, the actual bathymetry of the inlet exhibits fairly steep slopes. Since 1993, the sand spit has significantly retreated while the northern channel has opened up. The most spectacular retreats occur during storms. However, another mechanism of this recession is lateral erosion by the tidal current, extreme steepening of the banks and their subsequent collapse. The grid size smoothes the bathymetry in such a way that the banks will never appear steep. The 'oversteepening' process cannot therefore be reproduced by the model. As an example, the banks of the deepest channels in the inlet (20 m) will exhibit an apparent slope of 8% vs. an actual slope of 15% (Michel and Howa, 2000, personal communication).

The chosen strategy for input schematization is a major approximation, for two main reasons. (1) The use of average conditions throughout the year does not account for irreversible changes that may occur during storms, and that significantly affect the succeeding evolution of the inlet. (2) Representative wave conditions that would provide correct estimates of both longshore and cross-shore transports do not exist: the relationship between wave height and sediment transport cannot be simultaneously verified for both modes. We chose to account for longshore processes only in order to assess to what extent longshore sediment transport determines the long-term evolution of the inlet. Cross-shore processes, which play a determinant role in reshaping the outer delta of the inlet, were thus disregarded.

Our results confirm that a steady forcing is unlikely to reproduce the cyclic behavior of the inlet: the random occurrence of extreme events certainly drives 'catastrophic' morphological changes such as the breaching or complete remolding of sandbars. However, future applications of our model could include a more complex combination of tide and wave situations (such as the synchronization of spring tides with stormy weather, or the alternation of longer calm periods and extreme events). We think the use of a non-stationary forcing in this type of long-term morphological model would be worth investigating eventhough cross-shore processes might also have to be taken into account in order for the simulations to be more realistic.

Modeling the long-term morphological evolution of tidal inlets has been primarily based on two extreme strategies: (1) use of empirical relationships based on observations and similarities; and (2) development of process-oriented models, which consist in integrating small scale physics over large time scales. The cyclic behavior of the Arcachon tidal inlet places it among inherently unstable inlets (van de Kreeke, 1996), for which the use of empirical equilibrium relationships is questionable. On the other hand, physical models can only include some of the relevant physical processes (Capobianco et al., 1999), with an accuracy which not only depends on the limitation of computational capabilities, but also on the fundamental knowledge: sediment transport formulation, statistical nature of the input, importance of the chronology of events etc. (Southgate, 1995; van de Kreeke, 1996). Alternative solutions are found in the development of so-called behavior oriented models which combine the understanding of the behavior of the morphological unit (from observation or from simple process-oriented models) and mathematical models that exhibit the same behavior (van Dongeren and de Vriend, 1994; Capobianco et al., 1999). While these models may exhibit valuable prediction capabilities, process-based models remain a precious tool for a diagnostic approach, i.e. for a better understanding of the processes driving morphological evolution.

8. Conclusion

A 2DH morphodynamic process model has been developed in view of carrying out long-term simulations around a tidal inlet. The model reproduces several characteristics of observed inlet behavior such as the opening of a new channel and the drift of sand bodies across the inlet. The results are particularly promising when the model is run on an initially flat bathymetry since the combination of tidal currents and littoral drift leads to a configuration of the inlet similar to previously observed configurations. However, from a steady situation, such as the configuration reached after running the model on a flat bathymetry, the model cannot reproduce the opening of a new channel since this phenomenon most likely results from a breaching mechanism during extreme conditions (a storm during a spring tide, for instance (Friedrichs et al., 1993)). The migration of existing channels observed in the field might be due to secondary flows that are not accounted for in the model.

Long-term computations were achieved through a schematization of wave and tide conditions. The architecture of the Arcachon inlet is influenced by storms to a large extent, and a more refined modeling of its behavior would require the consideration of three-dimensional processes. Further validation of the model against data or theoretical cases is needed (application of the model to tide-dominated environments for instance). The use of several scenarios superimposing various tide and wave conditions is also worth investigating. The use of complex long-term morphodynamic models as predictive tools is not as yet performed; however, the integration of an input schematization method into a morphodynamic model as presented in this paper provides a complementary approach to developing behavior-oriented models.

Notations

a_0	amplitude of the orbital movement at the bottom
f	Coriolis parameter
f_w	wave friction factor
F_x, F_y	radiation stresses
g	gravity
h	water depth
H, H_s	wave height
M	number of velocity updates "by continuity"
N	number of tides per morphological time step
NH	number of morphological tides between full wave computations
p	porosity
p_{atm}	atmospheric pressure
$q(u_{tot},h)$	sediment transport formulation
T	tidal period
U,V	components along x and y of the vertically averaged velocity
u_{tot}	current velocity
z_0	roughness length
Δt_h	hydrodynamic time step
Δt_s	sedimentological time step
ΔT_m	morphological time step
ν	cinematic viscosity
ρ	water density
ρ_s	sediment density
τ_{bx},τ_{by}	bottom stress components along x and y
ζ	water surface elevation

References

Andersen, O.H., Hedegaard, I.B., Deigaard, R., de Girolamo, P., Madsen, P., 1991. Model for morphological changes under waves and current, Preprints IAHR, Symposium Suspended Sediment Transport, Florence, Italy, pp. 327–338.

Bellessort, B., Migniot, C., 1987. Catalog of sedimentary conditions along the French coasts. The English Channel and Atlantic coasts: Part C. From the Gironde Estuary to the Spanish border, Laboratoire Central d'Hydraulique de France, Maisons-Alfort (France). Collect. Dir. Etud. Rech. Electr. Fr. 75, 369–559.

Bijker, E.W., 1971. Longshore transport calculations. J. Waterw., Harbors Coastal Eng. Div. Am. Soc. Civ. Eng. 97 (WW4), 687–701.

Bondzie, C., Panchang, V.G., 1993. Effects of bathymetric complexities and wind generation in a Coastal Wave Propagation Model. Coastal Eng. 21, 333–366.

Bouchet, J.M., 1974. Evolution, hydrologie, écologie du Bassin d'Arcachon. Bull. I.G.B.A. 15, 15–30 (in French).

Briand, M.H.G., Kamphuis, J.W., 1993a. Sediment transport in the surf zone: a quasi 3D model. J. Coastal Eng. 20, 135–156.

Briand, M.H.G., Kamphuis, J.W., 1993b. Waves and currents on natural beaches: a quasi 3D model. J. Coastal Eng. 20, 101–134.

Bruun, P., 1978. Stability of tidal inlets, Theory and Engineering. Elsevier, Amsterdam, Netherlands, 510 pp.

Bruun, P., 1986. Morphological and navigational aspects of tidal inlets on littoral drift shores. J. Coastal Res. 2 (2), 123–143, Fort Lauderdale.

Bruun, P., Gerritsen, F., 1960. Natural bypassing of sand at coastal inlets. J. Waterw., Harbors Div. 85, 75–107.

Capobianco, M., de Vriend, H.J., Nicholls, R.J., Stive, J.F., 1999. Coastal area impact and vulnerability assessmnet: the point of view of a morphodynamic modeller. J. Coastal Res. 15 (3), 701–716.

Cayocca, F., 1996. Modélisation morphodynamique d'une embouchure tidale: Application aux passes d'entrée du Bassin d'Arcachon, PhD Thesis, University Bordeaux 1, France, 419 pp. (in French).

Chesher, T.J., 1995. Numerical morphodynamic modelling of Keta Lagoon. Proceedings Coastal Dynamics '95. pp. 927–937.

Chesher, T.J., Miles, G.V., 1992. The concept of a single representative wave for use in numerical models of long-term sediment transport predictions. In: Falconer, R.A., Chandler-Wilde, S.N., Liu, S.Q. (Eds.), Proc. 2nd International Conference on Hydraulic and Environment Modeling of Coastal, Estuaries and Rivers Waters, Bradford, Ashgate, Brookfield, VT. pp. 371–380.

Chesher, T.J., Wallace, H.M., Meadowcroft, I.C., Southgate, H.N., 1993. PISCES, A Morphodynamic Coastal Area Model, First Annual Report, Report SR 337, April 1993, HR Wallingford.

Coeffé, Y., Péchon, P., 1982. Modelling of sea-bed evolution under wave action. Proceedings 18th Conference ICCE, Capetown.

Damgaard, J.S., Latteux, B., Whitehouse, R.J.S., 1995. Sediment transport on sloping beds: a literature review, Report SR 404, HR Wallingford, 1995.

de Vriend, H.J., 1987a. 2DH Mathematical modelling of morphological evolution in shallow water. Coastal Eng. 11, 1–27.

de Vriend, H.J., 1987b. Analysis of horizontally two-dimensional morphological evolution in shallow water. J. Geophys. Res. 92 (C4), 3877–3893.

de Vriend, H.J., 1994. Two-dimensional horizontal and weakly three-dimensional models of sediment transport due to waves and currents. In: Abbott, M.B., Price, W.A. (Eds.), Coastal, Estuarial and Harbour Engineers' Reference Book. E&FN. Spon, London, pp. 215–238.

de Vriend, H.J., Copabianco, M., Chesher, T., De Swart, H.E., Latteux, B., Stive, M.J.F., 1993a. Long term modeling of coastal Morphology. Coastal Eng. 21, 225–269.

de Vriend, H.J., Zyserman, J., Nicholson, J., Roelvink, J.A., Péchon, P., Southgate, H.N., 1993b. Medium term 2DH coastal area modeling. Coastal Eng. 21, 193–224.

Deigaard, R., Fredsoe, J., Hedegaard, I., 1986a. Mathematical modeling for littoral drift. J. Waterw., Port, Coastal Ocean Eng., AM. SOC. CIV. ENG. 112 (3), 351–369.

Deigaard, R., Fredsoe, J., Hedegaard, I., 1986b. Suspended sediment in the surf zone. J. Waterw., Port, Coastal Ocean Eng., Am. Soc. Civ. Eng. 112 (1), 115–128.

Escoffier, F.F., 1977. Hydraulics and Stability of Tidal Inlets, General Investigation of Tidal Inlets (GITI), Rep. 13, US Army Corps of Engineers.

Fitzgerald, D.M., 1988. Shoreline erosional — depositional processes associated with tidal inlets. In: Aubrey, D.G., Weishar, L. (Eds.), Lecture Notes on Coastal and Estuarine Studies. Springer-Verlag, pp. 186–225.

Fredsoe, 1978. Sedimentation of river navigation channel. J. Hydraul. Div., Am. Soc. Civ. Eng. 104 (HY2), 223–236.

Friedrichs, C.T., Aubrey, D.G., Gies, G.S., Speer, P.E., 1993. Hydrodynamic modeling of a multiple-inlet estuary-barrier system: insight into tidal inlet formation and stability, formation and evolution of multiple tidal inlets. Coastal Estuarine Stud. 44, 95–112, AGU.

Gao, S., Collins, M., 1994. Tidal inlet stability in response to hydrodynamic and sediment dynamic conditions. Coastal Eng. 23, 61–80.

Gassiat, L., 1989. Hydrodynamique et évolution sédimentaire d'un système lagune-flèche littorale. Le Bassin d'Arcachon et la flèche du Cap Ferret. Thèse de doctorat, Université de Bordeaux I (in French).

Gerritsen, F., 1990. Morphological stability of tidal inlets and channels of the Western Wadden Sea, Rijkswaterstaat Report GWAO-90.019, the Netherlands.

Goodwin, P., 1996. Predicting the stability of tidal inlets for wetland and estuary management. J. Coastal Res., Spec. Issue 23, 83–102.

Gougenheim, A., 1953. Sur les fréquences des coefficients de marée. COEC 3, 119–133 (in French).

Hamm, L., Tanguy, J.M., Zhang, B., 1994. Prise en compte des effets gravitaires dans la modélisation du transport solide par charriage. Houille Blanche 4 (in French).

Hauguel, A., 1978. Utilisation de modèles mathématiques pour l'étude du transport solide sous l'action des courants de marée, Rapport EDF-LNH No. HE/42/78.41 (in French).

Hayes, M.O., 1980. General morphology and sediment patterns in tidal inlets. Sediment. Geol. 26 (1–3), 139–156.

Holthuijsen, L.H., Booij, N., Herberes, T.H.C., 1989. A prediction model for stationary, short-crested waves in shallow water with ambient currents. Coastal Eng. 13, 23–54.

Kamphuis, J.W., 1991. A long-shore sediment transport rate. J. Waterw., Port, Coastal Ocean Eng., Am. Soc. Civ. Eng. 117 (6), 624–640.

Kamphuis, J.W., 1992. Computation of coastal morphology, Design and Reliability of Coastal Structures, Venice.

Keulegan, G.H., 1951. Water-level fluctuations of basins in communication with seas, Third Progress Report on Tidal Flow in Entrances, Beach Erosion Board, Corps of Engineers, Department of the Army, U.S. Department of Commerce, National Bureau of Standards Report 1146A.

Komar, P.D., 1996. Tidal-inlet processes and morphology related to the transport of sediments. J. Coastal Res., Spec. Issue 23, 23–46.

L'Yavanc, J., 1995. Evolution bathymétrique et morphologique du Bassin d'Arcachon, Rapport Interne Ifremer DEL/95.12 Brest (in French).

Latteux, B., 1987. Modélisation du transport solide; Méthodologie à long-terme de l'évolution des fonds, Rapport LNH HE-42/87.25, 85 pp. (in French).

Latteux, B., 1995. Techniques for long-term morphological simulation under tidal action. Mar. Geol. 126, 129–141.

Lazure, P., Salomon, J.C., 1991. Numerical study of marine circulation between Quiberon and Noirmoutier. In: Chamley, H. (Ed.), Proceedings of the International Symposium on Environment of Epicontinental Seas, Lille. Oceanol. Acta, vol. 11, pp. 93–99.

LCHF (Laboratoire Central Hydraulique de France), 1969, Etude Hydraulique du Bassin d'Arcachon, Mission d'observations en nature, Rapport Général, Février 1969 (in French).

LCHF (Laboratoire Central Hydraulique de France), 1973, Etude Hydraulique du Bassin d'Arcachon, Mission d'observations complémentaires en nature, Rapport Général, Mars 1973 (in French).

Longuet-Higgins, M.S., Stewart, R.W., 1964. Radiation stresses in water waves, a physical discussion with applications. Deep-Sea Res. 11, 529–562.

Maruyama, K., Takagi, T., 1988. A simulation system of near-shore sediment transport for the coupling of the sea-bottom topography, waves and currents. Proc. IAHR, Copenhagen.

Michel, D., Howa, H., Tastet, J.P., 1995. Essai de modélisation de l'évolution morphologique d'un banc sableux intertidal (Sud du Bassin d'Arcacachon, France). CRAS 321, 497–501 (in French).

Michel, D., Howa, H., 1997. Morphodynamic behavior of a tidal inlet system in a mixed-energy environment. Phys. Chem. Earth 22, 339–343.

Michel, D., Howa, H., 2000. Evolution of a tidal inlet and interaction with adjacent coastline: Arcachon Inlet, south–west France. Mar. Geol. submitted for publication.

Nicholson, J., Broker, I., Roelvink, J.A., Price, D., Tanguy, J.M., Moreno, L., 1997. Intercomparaison of coastal area morphodynamic models. Coastal Eng. 37, 97–123.

O'Brien, M.P., 1931. Estuary tidal prisms related to entrance areas. Civ. Eng. 1 (8), 738–739.

O'Brien, M.P., 1969. Equilibrium flow areas of inlets in sandy coasts. J. Waterw., Harbors Coastal Eng. Div., Am. Soc. Civ. Eng. 95 (WW1), 43–52, February.

Ohnaka, S., Watanabe, A., 1990. Modeling of wave-current interaction and beach change. Proc. 22nd ICCE, Delft. pp. 2443–2456.

Orgeron, 1974. Sédimentologie des passes d'entrée du Bassin d'Arcachon. Bull. I.G.B.A. 15, 31–51 (in French).

Ranasinghe, R., Pattiaratchi, C., Masselink, G., 1999. A morphodynamic model to simulate the seasonal closure of tidal inlets. Coastal Eng. 27, 1–36.

Ribberink, J.S., Negen, E.H., Hartsuiker, G., 1995. Mathematical modelling, of coastal dynamics near a tidal inlet system. Proceedings Coastal Dynamics '95. pp. 916–926.

Roelvink, J.A., van Banning, G.K.F.M., 1994. Design and Development of Delft-3D and application to coastal morphodynamics. In: Verwey, A., Minns, A.W., Babovic, V., Maksimovic, M. (Eds.), Hydroinformatics '94. Balkema, Rotterdam, pp. 451–456.

Salomon, J.C., Breton, M., 1993. Arcachon: l'hydrodynamique par la modélisation mathématique, IFREMER Report (in French).

Soulsby, R.L., 1995. The "Bailard" sediment transport formula: comparison with data and models, MAST G8M Coastal Morphodynamics, Final Overall Meeting, Gdansk, Sept. 1995.

Soulsby, R.L., Hamm, L., Klopman, G., Myrhaug, D., Simons, R.R., Thomas, G.P., 1993. Wave-current interaction within and outside the bottom boundary layer. Coastal Eng. 21 (1–3), 41–69.

Southgate, H.N., 1995. The effects of wave chronology on medium and long-term coastal morphology. Coastal Eng. 26, 251–270.

Steijn, R.C., 1989. Voordelta morphological study, Schematization of the natural conditions in multi-dimensional numerical models of coastal morphology, Delft Hydraulics/Rijkswaterstaat, Rept. H526, February 1989.

Steijn, R.C., 1992. Input filtering techniques for complex morphological models, Delft Hydraulics, Report. H 824.53.

Steijn, R.C., Hartsuiker, G., 1992. Morphodynamic response of a tidal inlet after a reduction in basin area, Delft Hydraulics, Coastal Genesis report. H840.40, 75 pp.

Struiksma, N., Olewesen, K.W., Flokstra, C., de Vriend, H.J., 1985. Bed deformation in curved alluvial channels. J. Hydraul. Res. 23 (1).

Tanguy, J.M., Zhang, B., Hamm, L., 1993. A new Lax–Wendroff algorithm to solve the bed continuity equation with slope effect. 3rd International Conference on Estuarine and Coastal Modeling, Oak Brook, IL.

van de Kreeke, J., 1996. Morphological changes on a decadal time scale in tidal inlets: modeling approaches. J. Coastal Res., Spec. Issue 23, 73–82.

van Dongeren, A.R., de Vriend, H.J., 1994. A model of morphological behaviour of tidal basins. Coastal Eng. 22, 287–310.

Wang, Z.B., 1991. Morphodynamic Modeling for a tidal inlet in the Wadden Sea, Progress Report H840–50, Part II, Delft Hydraulics.

Wang, Z.B., 1992. Theoretical analysis on depth-integrated modeling of suspended sediment transport. J. Hydrol. Res. 30 (3).

Wang, Z.B., de Vriend, H.J., Louters, T., 1991. A morphodynamic model for a tidal inlet. In: Arcilla (Ed.), Computer Modeling in Ocean Engineering. Balkema, Rotterdam.

Wang, Z.B., Louters, T., de Vriend, H.J. et al., 1995. Morphodynamic modeling for a tidal inlet in the Wadden Sea. Mar. Geol. 126, 289–300.

Watanabe, A., 1982. Numerical models of near-shore currents and beach deformation. Coastal Eng., Jpn. 25, 147–161.

Watanabe, A., Maruyuma, K., Shimizu, T., Sakakiyama, T., 1986. Numerical prediction model of three-dimensional beach deformation around a structure. Coastal Eng., Jpn. 29.

Zyserman, J.A., Hedegaard, I.B., Fredsoe, J., Deigaard, R., 1991. Requirements to a sediment transport model for morphological modeling. In: Arcilla (Ed.), Computer Modeling in Ocean Engineering. Balkema, Rotterdam.